ACS APPLIED MATERIALS & INTERFACES

Research Article

www.acsami.org

Ultrathin Organic Solar Cells with Graphene Doped by Ferroelectric Polarization

Keumok Kim,[†,‡] Sang-Hoon Bae,[†] Chee Tat Toh,[§] Hobeom Kim,[⊥] Jeong Ho Cho,[#] Dongmok Whang,[‡] Tae-Woo Lee,[⊥] Barbaros Özyilmaz,*[,§] and Jong-Hyun Ahn*[,†]

[†]School of Electrical and Electronic Engineering, Yonsei University, Seoul 120-749, Korea

[‡]School of Advanced Materials Science and Engineering and [#]School of Chemical Engineering and SKKU Advanced Institute of Nanotechnology (SAINT), Sungkyunkwan University, Suwon 440-746, Korea

[§]Department of Physics, Graphene Research Centre and NanoCore, National University of Singapore, Singapore 117576

[⊥]Department of Materials Science and Engineering, Pohang University of Science and Technology, Pohang, Gyungbuk790-784, Korea

Supporting Information

ABSTRACT: Graphene has been employed as transparent electrodes in organic solar cells (OSCs) because of its good physical and optical properties. However, the electrical conductivity of graphene films synthesized by chemical vapor deposition (CVD) is still inferior to that of conventional indium tin oxide (ITO) electrodes of comparable transparency, resulting in a lower performance of OSCs. Here, we report an effective method to improve the performance and long-term stability of graphene-based OSCs using electrostatically doped graphene films via a ferroelectric polymer. The sheet resistance of electrostatically doped few layer graphene films was reduced to ~70 Ω/sq at 87% optical transmittance. Such graphene-based OSCs exhibit an efficiency of 2.07% with a superior stability when compared to chemically doped graphene-based OSCs. Furthermore, OSCs constructed on ultrathin ferroelectric film as a substrate of only a few micrometers show extremely good mechanical flexibility and durability and can be rolled up into a cylinder with 7 mm diameter.

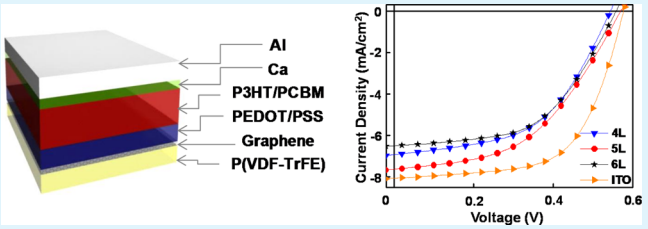

KEYWORDS: *graphene, organic solar cell, electrostatic doping, flexible electronics, transparent electrode*

1. INTRODUCTION

Organic solar cells (OSCs) have been widely recognized as an important energy-harvesting device because they are lighter, more flexible, and potentially cheaper than inorganic solar cells.[1−3] Indium−tin-oxide (ITO) films have been dominantly used in OSCs as an anode because of their high electrical conductivity, good optical transparency, and well-established manufacturing process. However, ITO thin films have drawbacks such as the diffusion of metal ions to the organic active layer, which degrades the performance of OSCs and leads to poor mechanical properties. This restricts their application in flexible OSCs.[4−6] Recently, graphene films grown by chemical vapor deposition have been explored as a potential ITO alternative because of their outstanding mechanical and optical properties and the possibility of mass production. Much effort has been devoted to overcoming the relatively low electrical conductivity of graphene that yields poor performance of OSCs, thereby restricting the range of possible applications. There are three general approaches for improving the electrical conductivity of graphene films: (i) electrostatic doping of graphene with ferroelectric polymers,[7] ii) "multilayer stack" method of graphene films[8−10] and (iii) "chemical doping" methods that use wet chemical dopants such as nitric acid,[11−13] tetracyanoquinodimethane (TCNQ),[14] and $AuCl_3$.[15] Combining the second and third method greatly improves the conductivity of graphene films, making it comparable to that of ITO.[16] Although this chemical doping is a very effective technique, most experiments rarely address the issue of sheet resistance stability. In fact, it is well-known that the adsorption of chemical molecules such as moisture and oxygen that exist under environmental conditions is unavoidable in the multilayer stack approach and over time significantly decreases the electrical conductivity of doped graphene films.[17] As a result, the long-term stability of OSCs incorporated with graphene electrodes is dramatically shortened to a few hours.

In this paper, we present our efforts in fabricating very flexible OSCs enabled with few layer graphene electrodes which are electrostatically doped by a layer of ferroelectric polymer coating, poly(vinylidene fluoride-co-trifluoroethylene) (P(VDF-TrFE)).[18,19] This nonvolatile electrostatic doping method by the remnant ferroelectric polarization of P(VDF-TrFE) effectively enhances the conductivity and stability of few

Received: November 21, 2013
Accepted: February 12, 2014
Published: February 12, 2014

layer graphene[7,20,21] and improves the lifetime of the resulting OSCs. In addition, the ferroelectric polymer film can be utilized both as a substrate and a doping layer simultaneously, with ultrathin film thickness via a solution process. OSCs can be constructed on only a few micrometer thick substrates including graphene electrodes, which can widen the device application area to various electronic devices and systems requiring very lightweight and high mechanical demand such as rollability.

2. EXPERIMENTAL SECTION

2.1. Electrode Fabrication. Monolayer graphene was grown on 25 μm thickness Cu foil using the well-known Chemical Vapor Deposition (CVD) method.[8] The Cu foil was placed inside a thermal CVD furnace at a pressure of 6.5×10^{-3} Torr. The temperature was then raised up to 1000 °C under 8 sccm of hydrogen gas (H_2) flow. After the temperature of the Cu foil reached 1000 °C, it was annealed for 30 minutes in order to increase the grain size of copper.[22,23] Next, while maintaining the temperature, 20 sccm of methane (CH_4) and 8 sccm of H_2 were passed through the furnace. After 30 minutes, the temperature was reduced to room temperature in a H_2 (8 sccm) atmosphere. To make multilayer graphene electrodes, poly(methyl methacrylate) (PMMA, Sigma Aldrich, molecular weight ~996 000) was used as supporting layer on graphene. The PMMA coated graphene obtained after etching of Cu foil in aqueous ammonium persulfate solution was transferred onto another graphene on Cu foil. The Cu foil acts as a temporary substrate, and this etch and transfer method was repeated to form a multilayer film. This method is good for reducing organic impurities like unremoved PMMA in between layers during the transfer of multi-layer graphene to the target substrate.[16] Next, P(VDF-TrFE) copolymer powder (65:35 mol %, Solvay Solexis) was dissolved in dimethylformamide (DMF) and coated on such multi-layer graphene on Cu foils after acetone removal of PMMA. P(VDF-TrFE) was annealed at 150 °C for 2 h to crystallize large ferroelectric β phase domains, which maximizes the ferroelectric properties of P(VDF-TrFE).[24,25] Subsequently, another monolayer graphene was transferred onto crystallized P(VDF-TrFE) and a voltage was applied to polarize the ferroelectric film. In a final step, Cu foil and graphene film attached to opposite side of P(VDF-TrFE) substrates for polarization were removed. To confirm the degree of polarization of the P(VDF-TrFE), P−V measurement was carried out. Figure S1 reveals the hysteresis loop of graphene/P(VDF-TrFE)/graphene structure under 150 V. The remnant polarization of P(VDF-TrFE) after polarized reaches 5.7 μC/cm^2 at 150 V. The doping effect of graphene was further examined by Raman spectroscopy.

2.2. Device Fabrication. The polarized graphene was transferred onto a supporting substrate and patterned by reactive ion etching (RIE) with O_2 plasma for use as an anode. The PEDOT: PSS (Clevios AI 4083 mixed with Zonyl FS-300 fluorosurfactant from Fluka[26,27]) was filtered with a 0.45 μm PVDF syringe filter and coated on top of the graphene electrode at 1000 rpm for 60 seconds then at 1500 rpm for 60 seconds. After the samples were dried on a hot plate at 130 °C for 20 minutes, they were moved into a glove box filled with Ar gas. The blended solution of poly(3-hexylthiophene) (P3HT, from Rieke Metals) and 1-(3-methoxycarbonyl)-propyl-1-phenyl-(6,6)C61 (PCBM, from Nano-C), each having a concentration of 20 mg/mL dissolved in dichlorobenzene (DCB) was used to make the bulk hetero junction (BHJ) structure. The solution was first filtered with a 0.2 μm PTFE syringe filter and coated over the PEDOT:PSS layer at 600 rpm for 135 s, then annealed at 130 °C for 30 min on a hot plate. Afterwards, 20 nm of Ca and 100 nm of Al were evaporated on the active layer by thermal evaporation (5×10^{-7} Torr) using a shadow mask. Finally, the fabricated devices were measured using a solar simulator under 100 mW/cm^2 with AM 1.5 G illumination conditions.

3. RESULTS AND DISCUSSION

The device structure of P3HT:PCBM bulk-heterojunction cell with electrostatically doped graphene electrode used in our measurements is shown in Figure 1a. This device has a thickness of less than 5 μm, with the spin coated P(VDF-TrFE) of 4 μm acting both as a doping layer for graphene and a substrate for the device. This enables impressive flexible performance for the device. During the fabrication process, the device was temporarily attached onto a rigid supporting substrate for ease of fabrication. After the device has been fabricated, it was detached from the supporting substrate (Figure 1b), and can then be transferred to any target surface (Figure 1c, d). The crystallinity of P(VDF-TrFE) film plays an important role in enhancing the electrostatic doping effect of graphene. The annealing process of the P(VDF-TrFE) film after coating on graphene enables the preferred crystal phase to form. This was observed in the characterized done by X-ray diffraction (XRD) (Figure 2a). The existence of the strong peak at 20° indicates the film consist of predominantly β phase which is required for its ferroelectric properties.[28,29] When an electric field is applied, the C−F dipoles align along the field direction where the net negative charge of the fluorine atoms is attracted to the positively biased graphene film. These non-volatile ferroelectric dipoles are polarized perpendicular to the plane of the graphene film and lower the sheet resistance by p-doping graphene.[7,20,21,30] Note that the doping effect is highly stable under ambient conditions because the dipoles will maintain their alignment without any reorientation over long durations. The doping effect of graphene was further examined by Raman spectroscopy (inset of Figure 2a). The shift in G peak from 1582.7 to 1591 cm^{-1} was seen in the Raman spectra of graphene after the polarization of the P(VDF-TrFE) film, verifying that graphene was p-doped. It is well-known that the optical transmittance of multilayered graphene films decreases linearly as a function of the number of stacked layer. To confirm this, we measured the transmittances of mono- to six-layered graphene films with UV−vis absorption spectroscopy (Figure 2b). The transmittance decreases from 96.9 to 83.7% for one to six layers, respectively, which is slightly darker than previous reports because of multilayer domains within the CVD grown graphene. The sheet resistance after the polarization of

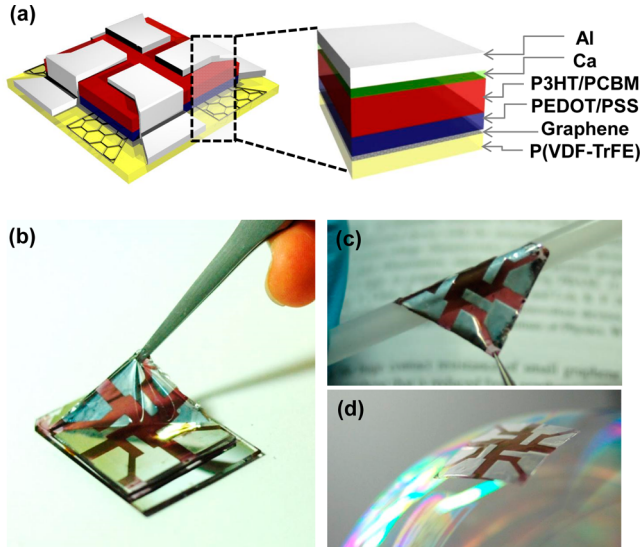

Figure 1. (a) Schematic diagram of BHJ OSC device with electrostatically doped graphene electrode. (b) Detaching fabricated OSC device from supporting substrate. (c, d) Attaching OSC device to target surface.

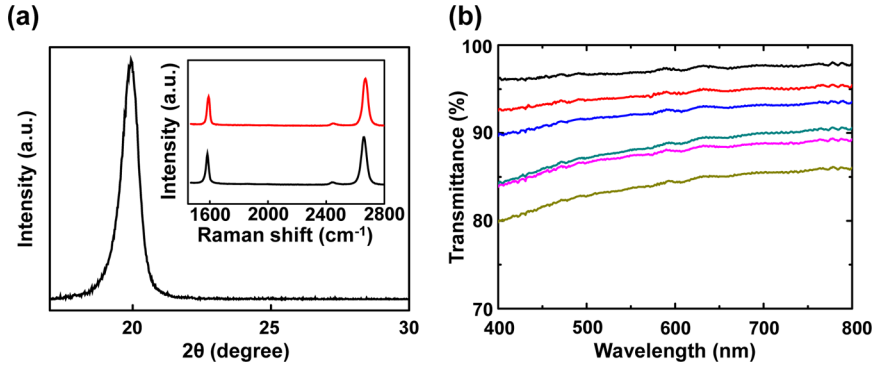

Figure 2. (a) XRD result of P(VDF-TrFE) film showing its crystallinity. Inset: Raman spectra of graphene films before and after polarization. (b) Optical transmittance of multilayered graphene films ranging from one (top) to six (bottom) layers.

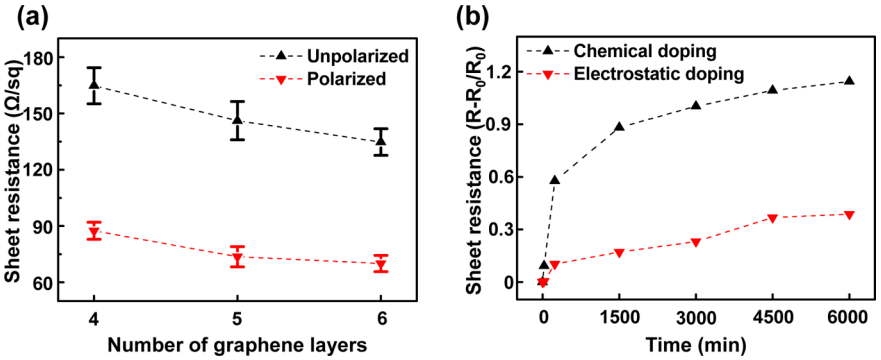

Figure 3. (a) Investigation of sheet resistance change with and without electrostatic doping for graphene stacks of 4–6 layers. (b) Comparison of stability for both chemically doped graphene film and electrostatically doped graphene film.

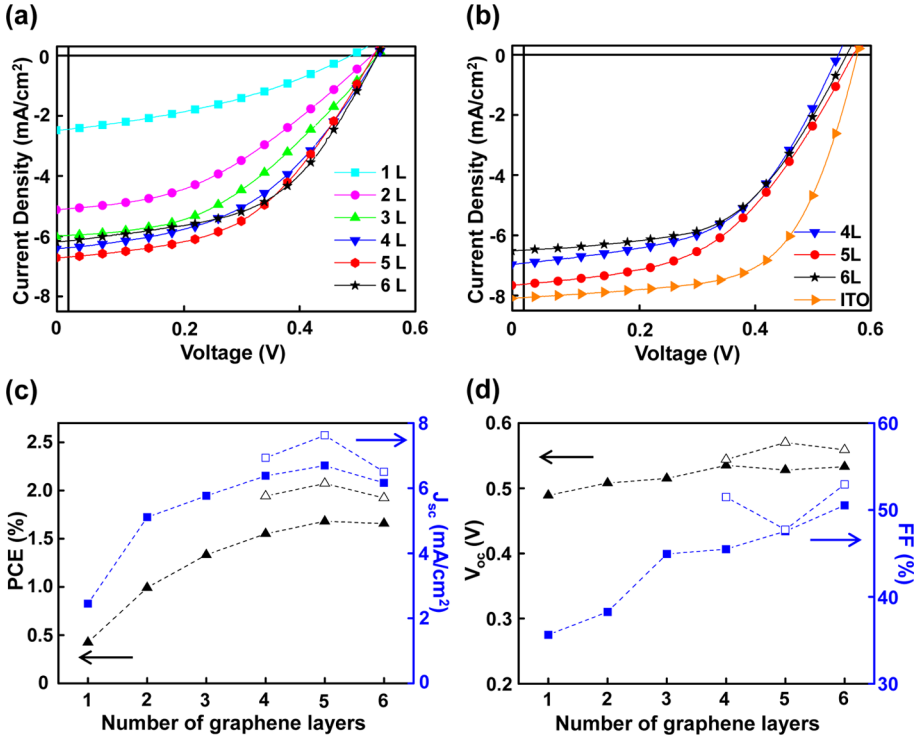

Figure 4. Performance of OSCs depending on sheet resistance enhancement. (a) *J*–*V* characteristics of stacked graphene electrode without polarization from 1 to 6 layers and (b) electrostatically doped 4 to 6 layer graphene electrodes and ITO. (c) Efficiency (triangle) and current density (square), (d) open circuit voltage (square) and fill factor (triangle) depending on the number of graphene layers and polarization. Filled symbols represent unpolarized characteristics, whereas opened symbols represent polarized characteristics.

dx.doi.org/10.1021/am405270y | ACS Appl. Mater. Interfaces 2014, 6, 3299–3304

Table 1. Summary of Detailed Photovoltaic Parameters with Layer by Layer Stacked Graphene and Electrostatically Doped Graphene to Enhance Sheet Resistance

no. of graphene layers	J_{sc} (mA/cm^2)	V_{oc} (V)	FF (%)	PCE (%)	sheet resistance (Ω/sq)	series resistance (Ω cm^2)	transmittance @550 nm (%)
1	2.45	0.489	35.62	0.43	421.41	110.78	96.9
2	5.09	0.525	39.04	1.04	245.33	58.55	94.2
3	5.97	0.534	41.96	1.34	190.33	43.89	92.1
4	6.38	0.535	45.49	1.55	164.78	30.03	88.1
	6.93[a]	0.544[a]	51.49[a]	1.94[a]	87.44[a]	22.70[a]	
5	6.69	0.528	47.56	1.68	146.15	28.82	87.5
	7.62[a]	0.570[a]	47.73[a]	2.07[a]	73.60[a]	27.74[a]	
6	6.16	0.533	50.53	1.66	134.73	28.51	83.7
	6.50[a]	0.559[a]	52.94[a]	1.92[a]	69.97[a]	26.67[a]	
ITO	8.07	0.577	61.53	2.86	15.00	12.35	

[a]Parameters after polarization.

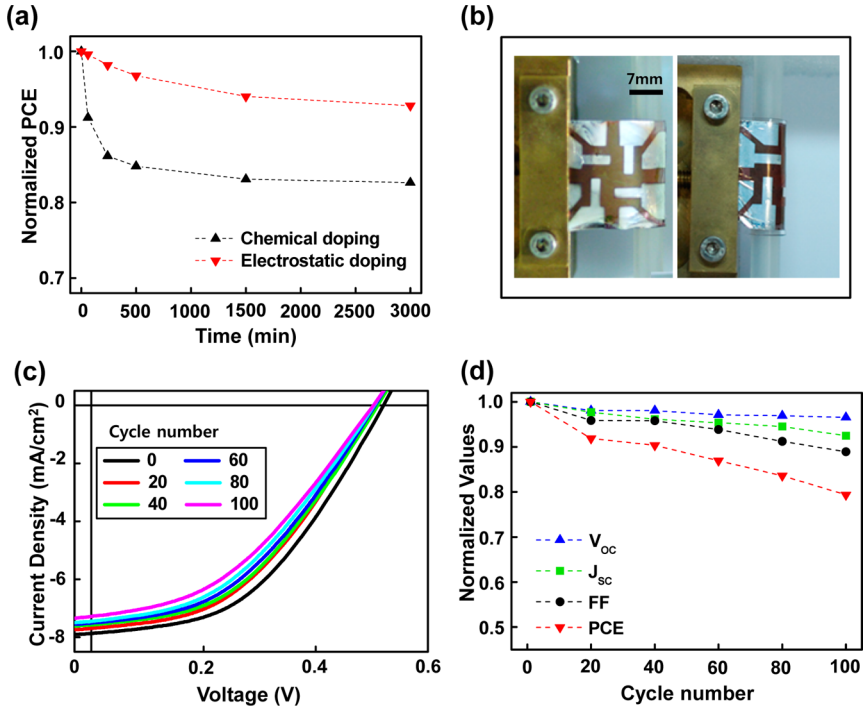

Figure 5. (a) Device stability with electrostatically doped and chemically doped graphene electrode as a function of time. (b) OSC device mounted on rollable machine for rolling test. (c) Changes in $J-V$ characteristics during cycling test. The $J-V$ curves are measured every 20 cycles. (d) Evaluation of normalized photovoltaic parameters under cycling test.

the P(VDF-TrFE) on four- to six-layer graphene films were measured (Figure 3a) and found to decrease between 47 and 50%. For example, the sheet resistance of the six-layer graphene film decreased from ∼135 to ∼70 Ω/sq. The issue of sheet resistance stability is important for any practical application, especially in OSCs, where it has a huge impact on efficiency. Comparison of sheet resistance stability for samples doped with nitric acid and polarized P(VDF-TrFE) film was studied over time (Figure 3b). The sheet resistance of the nitric-acid-doped graphene increased by 120% within 4 days of doping because of the volatile characteristics of nitric acid under ambient condition. On the other hand, the sheet resistance of electrostatically doped graphene increased by only 30% within the same duration after polarization. The stability is due to the ability of the ferroelectric dipoles to maintain their orientation in the polarized state over a long duration after polarization by an external field.

With ferroelectrically doped graphene anodes, we expect a significant performance enhancement in OSCs because of the combined improvement of electrical conductivity and long-term stability of the graphene electrodes. For formation of ferroelectrically doped graphene, a positive electric field was just applied to polarize P(VDF-TrFE) because this polarization direction consistently gave lower graphene sheet resistance than the other, and hence devices were all fabricated with this polarization for better performance. OSCs with one to six-layer stack of graphene were fabricated on unpolarized P(VDF-TrFE) and characterized. The open-circuit voltage (V_{oc}), short-circuit current (J_{sc}), fill factor (FF), and power conversion efficiency (PCE) were then extracted to evaluate the overall performance of the OSCs. Figure 4a shows the measured current density−voltage ($J-V$) characteristic of OSCs fabricated with one- to six-layer stack graphene films. The series resistance, which plays an important role in FF, was extracted from the inverse of the gradient of the $J-V$ curves at

V_{oc} and J_{sc}, respectively (Table 1). All devices have very similar tendency except for the monolayer graphene device, exhibiting much poorer efficiency than expected. This may be caused by microcracks and pinholes created during transfer process as well as its high sheet resistance.[31,32] In devices with up to four layers of graphene, the efficiency of cells tends to increase gradually with increasing graphene layer number. This result indicates that the improvement of the sheet resistance of graphene films dominantly affects the series resistance and FF in devices. On the other hand, graphene-based cells with even larger layer numbers display a performance saturation, with the six-layer cell (PCE ∼1.64%) showing lower efficiency than the five-layer cell (PCE ∼1.68%). Furthermore, the sheet resistance decreases less significantly with each additional graphene layer, which becomes more prominent at higher graphene carrier density (Figure 6). Thus, beyond four to five layers, the insignificant decrease in sheet resistance will no longer be beneficial for the OSCs since each additional graphene layer still reduces the transmittance by 2.3%; hence, we observe a reduction in efficiency of the OSCs with layer numbers exceeding five.

To investigate the effect of electrostatically doped graphene electrodes on the performance of OSCs, we measure $J-V$ characteristic of OSCs with four-, five-, and six-layered graphene electrodes after the polarization of P(VDF-TrFE) film. In addition, the photovoltaic performances of devices with ITO are included for comparison. The PCE is 1.94% and 2.07% for four- and five-layer graphene stack devices, respectively. This value decreased again to 1.92% for six layers, showing a similar trend as measured with undoped graphene devices. The device with five layer graphene exhibits J_{sc} of 7.62 mA/cm^2, FF of 47.73%, and PCE of 2.07%, which corresponds to an improvement of approximately 23% compared to the undoped five layer device. The overall performance of this device is still less than those with ITO electrodes. This is likely due to the much higher sheet resistance of the graphene electrode (∼73.6 Ω/sq), which results in higher series resistance for the device when compared with ITO electrode (∼20 Ω/sq). It is worthwhile to examine the effect of doped graphene layer number on the cell performance. The devices with four-, five-, and six-layer doped graphene electrodes show an improvement of PCEs by 25, 23, and 16%, respectively, as compared to undoped films (Figure 4 and Table 1). The improvements in PCE and other parameters tends to decrease gradually with the number of layers, which may result from the additional graphene layers screening the electrostatic potential created by the dipoles in P(VDF-TrFE) ferroelectric polymer. This effectively weakens the electrostatic doping effect on subsequent layers, reducing the improvement in sheet resistance.

OSCs with graphene doped electrostatically by ultrathin P(VDF-TrFE) substrate are expected to improve the long term stability of device performance and mechanical durability. To confirm these two characteristics, the change in PCE value and $J-V$ characteristics were measured as a function of time for stability and repeated rolling for durability of the device (Figure 5). The PCE value of OSCs fabricated on nitric acid doped graphene electrodes decreased by 17.4% within 2 days because of the volatile characteristics of nitric acid. On the other hand, the PCE of electrostatically doped graphene declined by only 7.2% after the polarization over the same period. The improved stability may be attributed to the fact that the ferroelectric dipoles can preserve their polarized state during long OSC operation and hence, maintain the improved sheet resistance of the graphene electrode (Figure 5a). In addition, this nonvolatile doping method is ideal for devices that are vulnerable to chemical dopants. These dopants, such as nitric acid, will react with active organic layers of device because of its volatile property and lead to device performance degradation. It is very important to have OSCs with good mechanical properties because one of the important applications for OSCs is flexible electronics.[5,13,26] In particular, the fabrication of rollable OSCs is very important to improve the portability of these devices. Such demand can be satisfied by utilizing an ultrathin substrate such as our solution processable P(VDF-TrFE) ferroelectric polymer. Figure 5b and c show the results of the mechanical rolling test using a rolling bar of 7 mm diameter and the $J-V$ curves obtained from the OSC device during repeated rolling test. Even when the device was rolled over 100 times, PCE changes only within the range of ∼21% and other factors including V_{oc}, J_{sc}, and FF declined by less than 11% (Figure 5d). Even though the variation range is large, there is plenty of room for improvement of device performance especially since this measurement was carried out under ambient condition without an encapsulation layer.

Next we relate the sheet resistance to the carrier density for non-volatile electrostatically doped graphene stacks of more than one layer.[7] The data in Table 1 is fitted with

$$T = \left(1 + \frac{Z_0}{2R_s}\frac{\sigma_{0p}}{\sigma_{DC}}\right)^{-2} \quad (1)$$

where, T is transmittance and R_s is sheet resistance. Z_0 is the impedance of free space and has the value of 377 Ω, $\sigma_{0p}/\sigma_{DC} = (e^2/4\hbar)/(ne\mu)$ is the ratio of the optical conductivity to DC conductivity.[33] A correction term is included to the fit to account for the electrostatic screening from each additional graphene layer as well. On this basis, the product of the monolayer graphene carrier density (n) and the carrier mobility (μ) is found to be 2.3 × 10^{16} V^{-1} s^{-1} for the four- to six-layer doped graphene stack devices. Currently, it is not possible to fabricate one- to three-layer doped graphene stack OSCs because of poor stack quality when less than three layers were used. This challenge arises from the graphene transfer process inducing cracks within the each graphene layer. Therefore, to highlight the potential of nonvolatile electrostatic doping with ferroelectric polymer, we include theoretical estimates for sheet resistance of one to three layers (Figure 6). It has been previously shown that with P(VDF-TrFE) electrostatic doping, a carrier density of up to 3 × 10^{13} cm^{-2} and carrier mobility of 2000 cm^2/(V·s) is possible for a large area CVD graphene

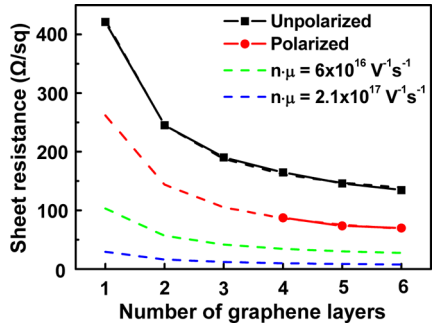

Figure 6. Experimental data (solid line) and theoretical estimate (dashed line) of R_s with layer number for different carrier density (n) and carrier mobility (μ) in the case of monolayer graphene.

dx.doi.org/10.1021/am405270y | ACS Appl. Mater. Interfaces 2014, 6, 3299−3304

device.[7] This results in $n\mu$ of 6×10^{16} V^{-1} s^{-1} corresponding to sheet resistance of 103, 42, and 30 Ω/sq with one, three and six layers respectively. Improvements in CVD graphene growth and transfer for better quality graphene with carrier mobility of 7000 $cm^2/(V{\cdot}s)$ is likely in the near future. This would makes values for $n\mu$ of 2.1×10^{17} V^{-1} s^{-1} and a sheet resistance of only 10 Ω/sq with four graphene layers possible. Tuning the work function of graphene is expected to further improve the overall efficiency of the OSCs, and is expected to be most significant in one- to two-layer graphene.

4. CONCLUSION

In summary, we demonstrated high-performance, rollable OSCs by utilizing the doping behavior in graphene because of the nonvolatile electrostatic potential created by the dipoles in P(VDF-TrFE) ferroelectric polymer. The device characteristics such as PCE and long-term stability exceeded those values in OSCs based on nitric-acid-doped graphene electrodes. This type of OSC fabricated with electrostatically doped graphene films without a chemical doping process provides a promising route to creating organic photovoltaic for future flexible applications.

■ ASSOCIATED CONTENT

Supporting Information

This material is available free of charge via the Internet at http://pubs.acs.org.

■ AUTHOR INFORMATION

Corresponding Authors

*E-mail: ahnj@yonsei.ac.kr.
*E-mail: phyob@nus.edu.sg.

Notes

The authors declare no competing financial interest.

■ ACKNOWLEDGMENTS

This work is supported by the Basic Research Program (2012R1A2A1A03006049 and 2009-0083540) and Global Frontier Research Center for Advanced Soft Electronics (2013M3A6A5073170) through the National Research Foundation of Korea (NRF), funded by the Ministry of Science, ICT and Future Planning and the Singapore National Research Foundation (NRF) through the Singapore-Berkeley Research Initiative for Sustainable Energy (SinBeRISE) CREATE Programme and Research Project NRF-RF2008-07, NRF-CRP9-2011-03, and the NUS Young Investigator Award.

■ REFERENCES

(1) Cheng, Y.-J.; Yang, S.-H.; Hsu, C.-S. *Chem. Rev.* **2009**, *109*, 5868−5923.
(2) Scharber, M. C.; Mühlbacher, D.; Koppe, M.; Denk, P.; Waldauf, C.; Heeger, A. J.; Brabec, C. J. *Adv. Mater.* **2006**, *18*, 789−794.
(3) Nelson, J. *Curr. Opin. Solid State Mater. Sci.* **2002**, *6*, 87−95.
(4) Kumar, A.; Zhou, C. *ACS Nano* **2010**, *4*, 11−14.
(5) Arco, L. G. D.; Zhang, Y.; Schlenker, C. W.; Ryu, K.; Thompson, M. E.; Zhou, C. *ACS Nano* **2010**, *4*, 2865−2873.
(6) Han, T.-H.; Lee, Y.; Choi, M.-R.; Woo, S.-H.; Bae, S.-H.; Hong, B. H.; Ahn, J.-H.; Lee, T.-W. *Nat. Photonics.* **2012**, *6*, 105−110.
(7) Ni, G.-X.; Zheng, Y.; Bae, S.; Tan, C. Y.; Kahya, O.; Wu, J.; Hong, B. H.; Yao, K.; Özyilmaz, B. *ACS Nano* **2012**, *6*, 3935−3942.
(8) Bae, S.; Kim, H.; Lee, Y.; Xu, X.; Park, J.-S.; Zheng, Y.; Balakrishnan, J.; Lei, T.; Kim, H. R.; Song, Y. I.; Kim, Y.-J.; Kim, K. S.; Özyilmaz, B.; Ahn, J.-H.; Hong, B. H.; Iijima, S. *Nat. Nanotechnol.* **2010**, *5*, 574−578.
(9) Kasry, A.; Kuroda, M. A.; Martyna, G. J.; Tulevski, G. S.; Bol, A. A. *ACS Nano* **2010**, *4*, 3839−3844.
(10) Li, X.; Zhu, Y.; Cai, W.; Borysiak, M.; Han, B.; Chen, D.; Piner, R. D.; Colombo, L.; Ruoff, R. S. *Nano Lett.* **2009**, *9*, 4359−4363.
(11) Jung, Y. U.; Na, S.-I.; Kim, H.-K.; Kang, S. J. *J. Vac. Sci. Technol., A* **2012**, *30*, 050604.
(12) Shin, D.-W.; Lee, J. H.; Kim, Y.-H.; Yu, S. M.; Park, S.-Y.; Yoo, J.-B. *Nanotechnology* **2009**, *20*, 475703.
(13) Lee, S.; Yeo, J.-S.; Ji, Y.; Cho, C.; Kim, D.-Y.; Na, S.-I.; Lee, B. H.; Lee, T. *Nanotechnology* **2012**, *23*, 344013.
(14) Hsu, C.-L.; Lin, C.-T.; Huang, J.-H.; Chu, C.-W.; Wei, K.-H.; Li, L.-J. *ACS Nano* **2012**, *6*, 5031−5039.
(15) Park, H.; Rowehl, J. A.; Kim, K. K.; Bulovic, V.; Kong, J. *Nanotechnology* **2010**, *21*, 505204.
(16) Wang, Y.; Tong, S. W.; Xu, X. F.; Özyilmaz, B.; Loh, K. P. *Adv. Mater.* **2011**, *23*, 1514−1518.
(17) Liu, H.; Liu, Y.; Zhu, D. *J. Mater.Chem.* **2011**, *21*, 3335−3345.
(18) Wen, F.; Xu, Z.; Tan, S.; Xia, W.; Wei, X.; Zhang, Z. *ACS Appl. Mater. Interfaces* **2013**, *5*, 9411−9420.
(19) Xia, W.; Xu, Z.; Zhang, Z.; Li, H. *Polymer* **2013**, *54*, 440−446.
(20) Zheng, Y.; Ni, G.-X.; Bae, S.; Cong, C.-X.; Kahya, O.; Toh, C.-T.; Kim, H. R.; Im, D.; Yu, T.; Ahn, J. H.; Hong, B. H.; Özyilmaz, B. *Europhys. Lett.* **2011**, *93*, 17002.
(21) Zheng, Y.; Ni, G.-X.; Toh, C.-T.; Zeng, M.-G.; Chen, S.-T.; Yao, K.; Özyilmaz, B. *Appl. Phys. Lett.* **2009**, *94*, 163505.
(22) Li, X.; Magnuson, C. W.; Venugopal, A.; An, J.; Suk, J. W.; Han, B.; Borysiak, M.; Cai, W.; Velamakanni, A.; Zhu, Y.; Fu, L.; Vogel, E. M.; Voelkl, E.; Colombo, L.; Ruoff, R. S. *Nano Lett.* **2010**, *10*, 4328−4334.
(23) Li, X.; Cai, W.; An, J.; Kim, S.; Nah, J.; Yang, D.; Piner, R.; Velamakanni, A.; Jung, I.; Tutuc, E.; Banerjee, S. K.; Colombo, L.; Ruoff, R. S. *Science* **2009**, *324*, 1312.
(24) Xia, W.; Xu, Z.; Zhang, Q.; Zhang, Z.; Chen, Y. *J. Polym. Sci., Part B: Polym. Phys.* **2012**, *50*, 1271−1276.
(25) Tanaka, R.; Tashiro, K.; Kobayashi, M. *Polymer* **1999**, *40*, 3855−3865.
(26) Kaltenbrunner, M.; White, M. S.; Głowacki, E. D.; Sekitani, T.; Someya, T.; Sariciftci, N. S.; Bauer, S. *Nat. Commun.* **2012**, *3*, 770.
(27) Lipomi, D. J.; Tee, B. C.-K.; Vosgueritchian, M.; Bao, Z. *Adv. Mater.* **2011**, *23*, 1771−1775.
(28) Chen, S.; Yao, K.; Tay, F. E. H.; Chew, L. L. S. *J. Appl. Polym. Sci.* **2010**, *116*, 3331−3337.
(29) Zhang, Q.; Xia, W.; Zhu, Z.; Zhang, Z. *J. Appl. Polym. Sci.* **2013**, *217*, 3002−3008.
(30) Bae, S.-H.; Kahya, O.; Sharma, B. K.; Kwon, J.; Cho, H. J.; Özyilmaz, B.; Ahn, J.-H. *ACS Nano* **2013**, *7*, 3130−3138.
(31) Cox, M.; Gorodetsky, A.; Kim, B.; Kim, K. S.; Jia, Z.; Kim, P.; Nuckolls, C.; Kymissis, I. *Appl. Phys. Lett.* **2011**, *98*, 123303.
(32) Choi, Y.-Y.; Kang, S. J.; Kim, H.-K.; Choi, W. M.; Na, S.-I. *Sol. Energy Mater. Sol. Cells* **2012**, *96*, 281−285.
(33) De, S.; Coleman, J. N. *ACS Nano* **2010**, *4*, 2713−2720.